https://doi.org/10.1016/j.jclepro.2021.128421

Influence of ternary blended cementitious fillers in a cold mix asphalt mixture

Dong Lu [a, b, #], Jian Yuan [c, #], Zhen Leng [d, *], Jing Zhong [a, b, *]

[a] *School of Civil Engineering, Harbin Institute of Technology, Harbin, 150090, PR China*
[b] *Key Lab of Structures Dynamic Behavior and Control of the Ministry of Education (Harbin Institute of Technology), Harbin, 150090, PR China*
[c] *Academy of Combat Support, Rocket Force University of Engineering, Xi'an, 710025, PR China*
[d] *Department of Civil and Environmental Engineering, The Hong Kong Polytechnic University, Hong Kong 999077, PR China*

* *Corresponding author e-mail addresses: zhen.leng@polyu.edu.hk (Z. Leng); zhongjing@hit.edu.cn (J. Zhong).*

 # These authors contributed equally to this work.

Abstract

The manufacture of conventional hot mix asphalt (HMA) for paving has a substantial environmental footprint, and the production of clean asphalt mixture with good engineering performance is critically important. The introduction of cementitious filler is a promising approach to achieve outstanding mechanical properties for cold mix asphalt (CMA) as a clean paving material. This study aims to develop a novel CMA formulation through the combination of ordinary Portland cement (OPC) with two industrial by-products: fly ash (FA) and ground-granulated blast furnace slag (GGBS), which could make CMA even cleaner. To achieve this objective, the effects of ternary blended cementitious fillers on the early-age strength, engineering performance, and microstructural properties of CMA are characterized through comprehensive laboratory tests. The experimental results indicated that the indirect tensile strength of CMA-B containing 2% OPC, 1% FA, and 1% GGBS is approximately 20% higher than that of the mixture with 2% OPC (CMA-2% OPC). The residual Marshall stability ratio of CMA-B was increased to about 95% and its dynamic stability was approximately 10 times that of CMA-2% OPC. Employing blended cementitious fillers in CMA facilitates the formation of hydration products with excellent stiffness, reduces the air voids, and enhances interface bonding between aggregate and asphalt matrix, and thus suitable for

applications in road pavements subjected to harsh service conditions in terms of moisture and temperature.

Keywords

Cleaner paving mixture; Cold mix asphalt; Cementitious fillers; Engineering performance; Microstructure

HIGHLIGHTS

- A novel CMA formulation incorporating ternary blended cementitious fillers (TBCF) was developed.
- Optimized combination (2% OPC, 1% FA, and 1% GGBS) of CMA was identified.
- The dynamic stability of the mixture with 2% OPC, 1% FA, and 1% GGBS was approximately 10 times that of CMA-2% OPC.
- Combined OPC, FA, and GGBS reduced the air voids, improved the interface, and produced a dense microstructure.

Abbreviations

CMA	Cold Mix Asphalt
HMA	Hot Mix Asphalt
GGBS	Ground-granulated Blast furnace Slag
C-S-H	Calcium-Silicate-Hydrate
SEM	Scanning Electron Microscopy
XRD	X-ray Diffraction
FTIR	Fourier Transform Infrared Spectrometer
CH	Calcium Hydroxide
TBCF	Ternary Blended Cementitious Fillers
OPC	Ordinary Portland Cement
FA	Fly Ash

1. Introduction

Routine maintenance and emergency repair can be implemented through hot mix asphalt (HMA) or cold mix asphalt (CMA) (Doyle et al., 2013; Ferrotti et al., 2014; Saadoon et al., 2018). Although HMA provides higher strength than CMA (Dulaimi et al., 2017; Moghadas Nejad et al., 2017), the manufacture of HMA has a substantial environmental footprint, due to the relatively high application temperature for the heating of bitumen and aggregate which causes a lot of fuel consumption (Dong et al., 2018; Dulaimi et al., 2020; Lin et al., 2017). Meanwhile, health and safety issues are created during the heating process (Nassar et al., 2016; Saadoon et al., 2018; Tian et al., 2020b). Currently, CMA has gradually aroused widespread interest in modern civil engineering (Ling et al., 2016; Martínez-Echevarría et al., 2012; Zhu et al., 2019a), because it is applied at ambient temperature and the micro-surfacing does not require a rolling compaction process (Yan et al., 2019; Zhu et al., 2019b). As such, CMA is a viable and environmentally sustainable substitute for HMA and can trigger a substantial economic benefit and alleviate its undesirable impacts on the ecological environment.

CMA is typically produced with asphalt emulsion, aggregate, filler, and water (Ayar, 2018; Diaz, 2016; Dong et al., 2018). Note that water is needed to set the cementitious part in asphalt as the cement powder does not react with the functional groups of the asphalt binder. In contrast to HMA, both environmental and economic benefits can be achieved by eliminating the need of heating substantial volumes of aggregate (Du, 2018; Dulaimi et al., 2017). However, the application of CMA is still limited, mainly due to its high air voids (Dulaimi et al., 2016), low early-age strength (Tian et al., 2020a), and high water sensitivity (Dodds et al., 2017; Dulaimi et al., 2020).

To address these issues and promote the application of CMA, the replacement of traditional

limestone filler (LF) with Portland cement has been widely utilized to manufacture CMA to obtain an acceptable early-age strength (Al-Khateeb and Al-Akhras, 2011; Bołtryk and Małaszkiewicz, 2013; Tian et al., 2020a). Filler, as one of the raw materials in asphalt mixture, mainly fills the air voids and reduces the gap between aggregates (Dulaimi et al., 2020; Lu et al., 2020), which plays a major role in controlling the performance of the mixture (Leandri et al., 2015; Mignini et al., 2021; Nassar et al., 2016). As such, proper selection of fillers and their combinations has been considered as an effective strategy to improve the performance of CMA. For instance, it has reported that replacing LF with cementitious binders can significantly affect the strength (Mignini et al., 2021; Saride et al., 2016), stiffness (Dołżycki et al., 2017; Nassar et al., 2016), and indirect tensile stiffness modulus (Dong et al., 2018; Xiao et al., 2019) of CMA. Additionally, to reduce cement consumption and carbon emission, a small amount of research has tried to mix active industrial by-products to replace the LF in CMA (Doyle et al., 2013; Dulaimi et al., 2016, 2017; Dulaimi et al., 2020). Fly ash (FA) and ground granulated blast furnace slag (GGBS), two commonly used active mineral admixtures, have shown great potential to improve the strength of CMA due to their filler effect and pozzolanic effect (Dulaimi et al., 2017; Ge et al., 2015). For example, Nassar et al. (2016) developed a CMA mixture using 80% GGBS and 20% cement (C-GGBS), and they found that the indirect tensile stiffness modulus of the C-GGBS mix cured at 20 ℃ for 7 days was approximately 13 times higher than that of the reference mixture with 100% LF.

According to the published literature, the influence of blended cementitious fillers on the engineering performance (e.g., moisture susceptibility, rutting resistance, and cracking resistance), and microstructure of CMA have not been sufficiently investigated. Additionally, high-performance CMA with excellent early-age strength and outstanding water stability has not yet been developed,

thereby hindering its practical applications in the requirement of rapid open traffic from an engineering performance perspective. To this end, this laboratory study aims to develop a novel CMA mixture via the combination of OPC with two industrial by-products: FA and GGBS, which are anticipated to make CMA even cleaner. The early road performance of CMA was conducted through early-age strength and engineering performance tests. Secondary electron imaging (SEI) and energy-dispersive spectrometers (EDS) in scanning electron microscope (SEM) analysis, Fourier transform infrared spectrometer (FTIR), and X-ray diffraction (XRD) were employed to shed light on the roles of the admixed fillers in CMA mixture. The findings of this study contribute to a deeper and more systematic understanding of the roles of the blended cementitious fillers in a CMA mixture, as well as better design and production of CMA with outstanding performance.

2. Materials and methods

2.1. Materials

To promote the deformation capability and flexibility of the CMA mixture, a commercial cationic asphalt emulsion was selected in this study. The properties of asphalt emulsion were tested according to the *Test Procedure for Highway Engineering Asphalt and Asphalt mixture (JTG E20-2011)* and summarized in Table 1. This type of asphalt emulsion has been extensively applied in routine maintenance and emergency repair due to its high stability (Nassar et al., 2016; Yan et al., 2014). Moreover, this type of asphalt emulsion can well coat aggregate and provide high adhesion.

Table 1 Properties of asphalt emulsion.

Test items	Evaporation residue				1.18 sieve test (%)
	Penetration (25 °C, 100 g, 5 s) (0.1 mm)	Soften point (°C)	Ductility (15 °C) (cm)	Content (%)	
Test value	86	53	80	60	0.05
Specification	80-100	≥50	≥40	-	-

Three types of cementitious fillers were used to replace the traditional limestone filler (LF) to manufacture the CMA mixture, including ordinary Portland cement of grade 42.5 (OPC), fly ash (FA), and granulated blast furnace slag powder (GGBS). The chemical compositions of the cementitious fillers were measured by X-ray fluorescence (XRF, Persee, China) analysis and presented in Table 2. As suggested by the particle size distribution analysis, the GGBS had the smallest size (Fig. 1). Table 3 and Table 4 list the physical properties of aggregate and LF, respectively. Fig. 2 shows the gradation curve of aggregate (coarse and fine) used to manufacture the CMA mixture, which met the requirements of the *Test Methods of Aggregate for Highway Asphalt Pavement (JTG E42-2005).*

Table 2 Chemical composition of the cementitious fillers (wt%).

Oxides	CaO	SiO_2	Al_2O_3	Fe_2O_3	SO_3	Loss on ignition
OPC	63.2	22.5	6.2	5.2	2.1	1.6
FA	6.7	28.5	19.2	8.5	0.5	6.1
GGBS	33.5	34.2	12.7	0.5	1.6	2.8

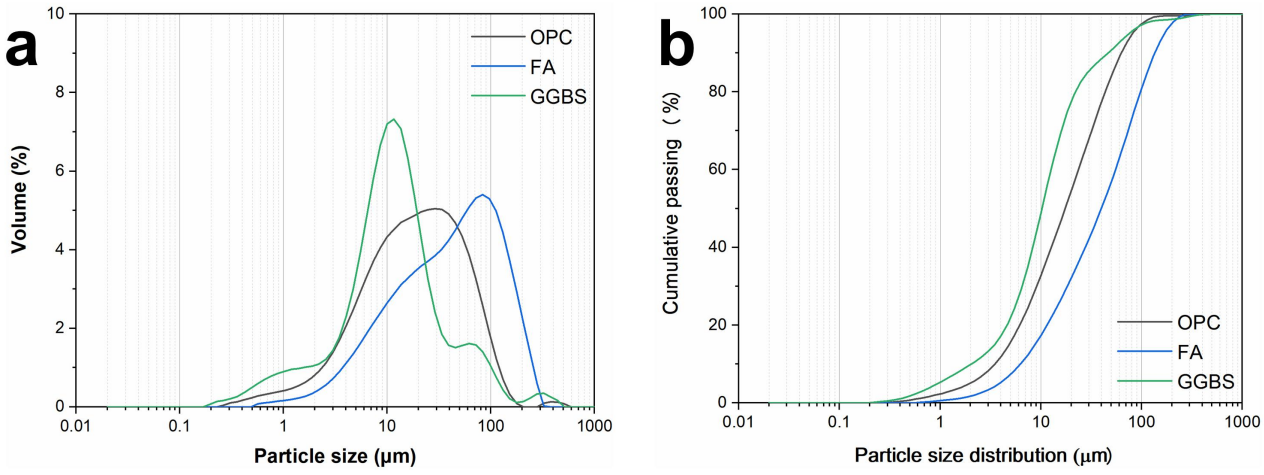

Fig. 1. Particle size distribution of cementitious fillers: (a) volume and (b) cumulative passing.

Table 3 Physical properties of aggregate.

Type	Water absorption (%)	Crushed index (%)	Apparent density (g/cm^3)	Bulk particle density (g/cm^3)
Coarse	0.51	18.73	2.766	2.58
Fine	1.73	-	2.738	2.47

Table 4 Properties of limestone filler.

Test items	Moisture content (%)	Specific surface area (m^2/kg)	Grain size distribution of limestone filler (%)		
			< 0.300 mm	< 0.150 mm	< 0.075 mm
Test value	0.92	325	100	95	80

129

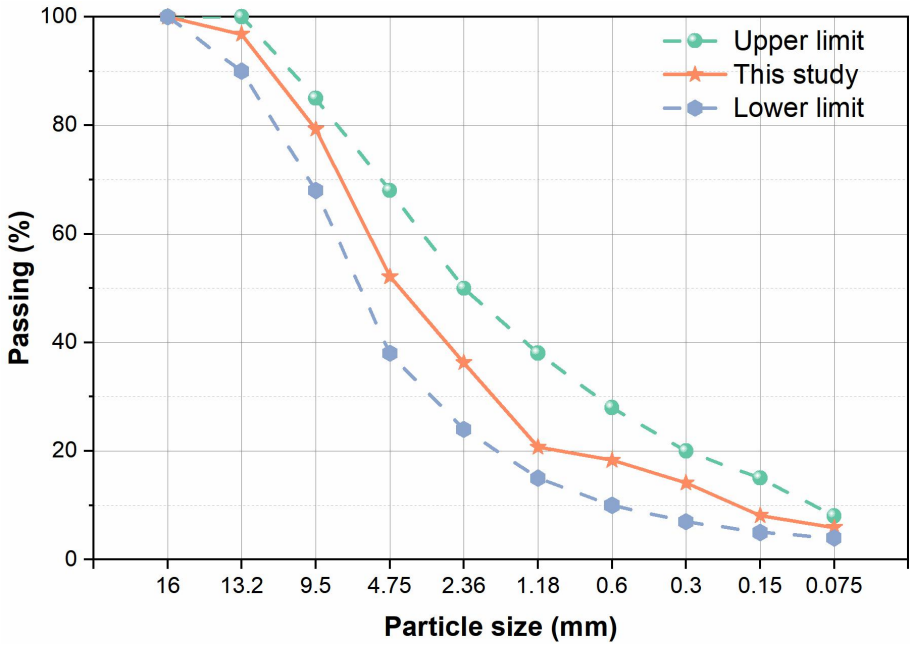

Fig. 2. Gradation curve of aggregate (coarse and fine) for mixture manufacture.

130 *2.2. Preparation of CMA samples*

131 In this study, seven CMA formulations were developed to investigate the possible roles of the
132 blended cementitious fillers in the CMA mixture. A performance-based composition method was
133 used to optimize the CMA proportion, as recommend by Dulaimi et al. (2020). In particular, the
134 CMA samples were prepared with 8 wt% asphalt emulsion (by weight of aggregate) and 6 wt%
135 fillers (by weight of aggregate), according to the experimental research results and common
136 experience (Dulaimi et al., 2017; Dulaimi et al., 2020; Tian et al., 2020a). Table 5 shows the mix
137 proportions of the CMA samples. The schematic representation of the fabrication of the Marshall
138 specimen is presented in Fig. 3. In particular, the weighed fine aggregate and coarse aggregate were
139 first mixed in a mechanical mixer (BH20, 20 L, China) for 120 s to obtain a homogeneous mixture.

Next, water and asphalt emulsion were added to the dry aggregate. Subsequently, filler was added to the mixture. Note that the content of asphalt emulsion and filler are by weight of the dry aggregate (fine and coarse). Finally, the fresh mixture was cast in the molds and compacted 50 times on each side using a Marshall compactor, and then cured at a temperature of 20 ℃ and humidity of 50% according to *Test Procedure for Highway Engineering Asphalt and Asphalt mixture (JTG E20-2011)*.

Table 5 Mix proportions of CMA mixtures.

Mixture ID	Asphalt emulsion (%)	Cementitious fillers combinations (%)				Aggregate (kg/m^3)	Water (kg/m^3)
		OPC	FA	GGBS	LF		
CMA-LF	8	0	-	-	6	1860	30
CMA-2% OPC	8	2	-	-	4	1860	30
CMA-4% OPC	8	4	-	-	2	1860	30
CMA-6% OPC	8	6	-	-	0	1860	30
CMA-A	8	2	0.5	1.5	2	1860	30
CMA-B	8	2	1	1	2	1860	30
CMA-C	8	2	1.5	0.5	2	1860	30

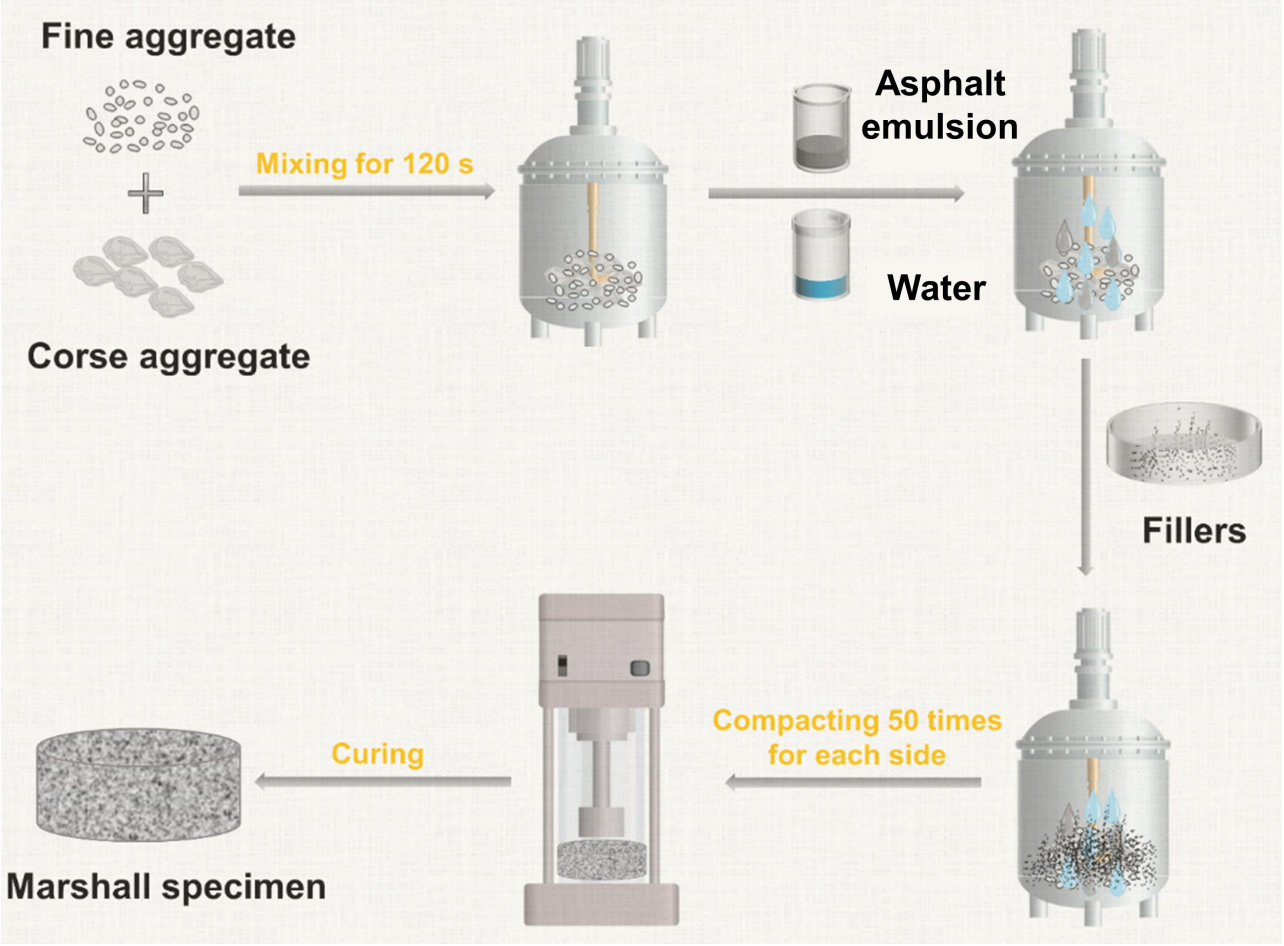

Fig. 3. Schematic illustration of CMA fabrication was illustrated by the example of the Marshall specimen.

148 *2.3. Testing methods*

149 The testing procedures of CMA specimens are presented in Fig. 4. First, the early-age strength of
150 the mixtures was assessed by indirect tensile strength (ITS) and raveling loss tests. Then, the
151 engineering performance was evaluated by moisture susceptibility, rutting resistance, and cracking
152 susceptibility tests. Finally, the microstructural properties of CMA were characterized by XRD,
153 FTIR, and SEM-EDS techniques.

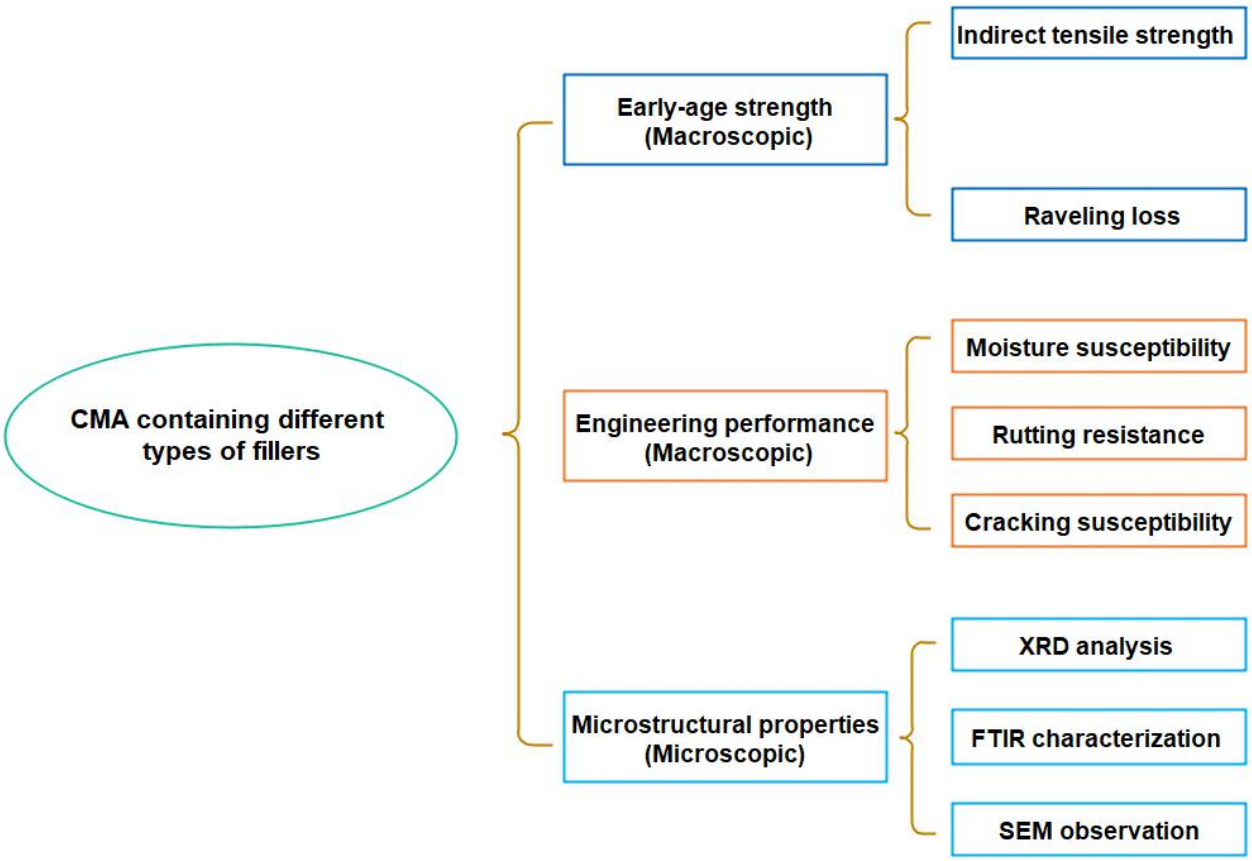

Fig. 4. Experimental plans and testing procedures.

154 *2.3.1. Early-age strength test*

155 Indirect tensile strength and raveling loss tests were conducted to evaluate the early-age strength of
156 CMA samples according to *ASTM D6931-17 (2017)* and *ASTM D7196-06 (2017)*, respectively. In
157 the indirect tensile test, the Marshall specimens (101.6 mm in diameter and 63.5 mm in height)
158 were prepared for tests at 20 ℃. The raveling test was performed to simulate the abrasion of CMA
159 caused by early-age traffic, as recommended by Yan et al. (Yan et al., 2017). In the raveling test, the
160 CMA samples (101.6 mm in diameter and 70 mm in height) were first prepared. Then, the raveling
161 test was continued for 15 min or until a major part of the specimens were broken. Finally, the
162 surface of the specimen was brushed to remove any loose parts. The average of three replicates was
163 recorded to assess the raveling loss.

164 *2.3.2. Engineering performance tests*

165 *1) Moisture susceptibility test*

166 According to th*e Test Procedure for Highway Engineering Asphalt and Asphalt mixture (JTG*
167 *E20-2011),* immersion Marshall and freeze-thaw (F-T) splitting tests were adopted to assess the
168 moisture susceptibility of CMA samples. The CMA samples for these two tests were 101.6 mm in
169 diameter and 63.5 mm in height and divided into two groups for each test.

170 In the immersion Marshall test, the CMA samples in group A were placed in a water bath at 60 ℃
171 for 48 h, whereas the samples in group B were socked in a water bath at 60 ℃ for 30-40 min. Four
172 replicates were prepared for each group to assess the residual Marshall stability ratio (RS, %) of the
173 CMA mixture. In the F-T splitting test, the CMA samples in group A were cured at room
174 temperature, whereas the specimens in group B were cured in a chamber at -18 ℃ for 16 h and then
175 placed in a water bath at 60 ℃ for 24 h. Finally, both groups of samples were soaked in a water bath
176 at 25 ℃ for 2 h. The loading speed was set as 50 mm/min. The average of four replicates was
177 recorded to evaluate the indirect tensile strength ratio (TSR, %) of the CMA mixture.

178 *2) Rutting resistance test*

179 An asphalt mixture rutting tester was adopted to assess the rutting resistance of the CMA mixture at
180 the high temperature according to *Test Procedure for Highway Engineering Asphalt and Asphalt*
181 *mixture (JTG E20-2011)*. The CMA slabs (300 mm × 300 mm × 50 mm) were cured with the mold
182 and placed in a chamber at 60 ℃. The specimens were then placed in the rutting tester with a wheel
183 pressure of 0.7 MPa to start the test. The average of three replicates was recorded to assess the
184 dynamic stability (*DS*, cycle/mm) of the CMA mixture.

3) Low-temperature cracking susceptibility

A three-point bending test was used to assess the low-temperature characteristics of the asphalt mixture according to *Test Procedure for Highway Engineering Asphalt and Asphalt mixture (JTG E20-2011)*. The beam specimens (250 mm × 30 mm × 35 mm) were first prepared from a slab specimen. Then, a UTM-100 universal testing machine was adopted to evaluate the ability of CMA specimens to resist cracking at low-temperature. The temperature was set at -10 ℃ and the loading rate was 50 mm/min. Based on the three-point bending test, the bending strength, bending failure strain, and bending creep stiffness were obtained to evaluate the cracking susceptibility of CMA at low-temperature.

2.3.3. Microstructure measurements

XRD (SmartLab, Rigaku, Japan) and FTIR (BRUKER TENSOR II, Germany) were adopted to analyze the composition of the CMA mortars. For this purpose, the dry powders (a uniform fineness of less than 45 μm) were produced by grinding the selected crushed mortar. XRD measurements were performed with Cu K_α radiation (λ=1.54 Å) and carried out using constant pass energy (40 kV and 35 mA). The diffraction patterns were obtained in the 2θ range of 15-65 degrees. The FTIR was performed with a wavenumber range of 400-4000 cm^{-1}. SEM-EDS (ZEISS Gemini 300, Germany) was used to reveal the morphology of the CMA. For this purpose, the collected samples were immersed in ethanol to stop hydration. Subsequently, they were dried at 60 ℃ for 48 h. At last, the surface of the specimens was sprayed with gold to increase conductivity before testing.

3. Results and discussion

3.1. Early-age strength

206 The early-age strength of the CMA mixture can directly affect its practical applications in the
207 requirement of rapid open traffic. As such, indirect tensile strength and raveling loss tests were
208 employed to gain in-depth insight into the early-age strength of the CMA mixture.

209 *3.1.1. Indirect tensile strength*

210 Fig. 5 displays the ITS values of the CMA samples containing different types of fillers. It can be
211 observed that the CMA-4% OPC sample demonstrated a higher ITS value, as compared to the
212 CMA-2% OPC sample or CMA-6% OPC sample. A similar beneficial role of the admixing cement
213 on the ITS was found in another study (Xiao et al., 2019), in which the addition of 3 wt% cement
214 increased the ITS of the mixture by about 30%. Using the ternary blended cementitious fillers could
215 further increase the ITS value. Especially for the CMA-B sample, there is an increase of
216 approximately 50% and 4% over the ITS of the CMA-LF mix and the CMA-4% OPC mix,
217 respectively. Indeed, the combined usage of cementitious fillers has been recently reported as
218 capable of enhancing the density and reducing the voids of CMA (Dulaimi et al., 2020), which was
219 mainly attributed to the formation of additional hydration products that filled the air voids. That is,
220 the pozzolanic reaction of the admixed cementitious fillers could consume a certain content of
221 calcium hydroxide (CH) crystals with lower strength and generate a large amount of calcium
222 silicate hydrate (C-S-H) phase in the interface area (see Fig. 6). In addition, the accelerated
223 demulsification of asphalt emulsion induced by the existence of cementitious materials could also
224 enhance the strength of CMA (Dolzycki et al., 2017; Dołżycki et al., 2017).

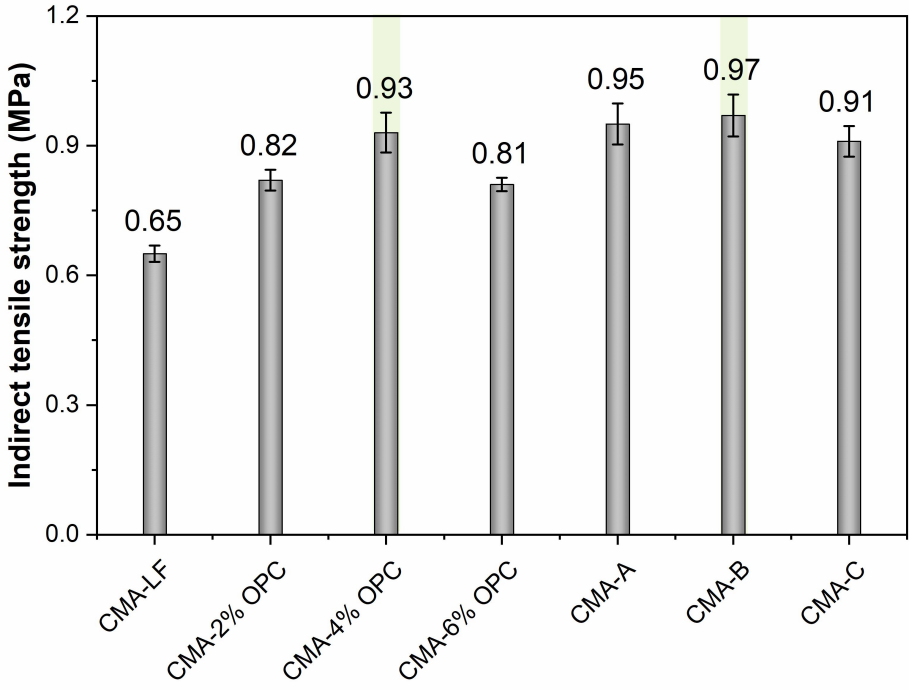

Fig. 5. Indirect tensile strength of the CMA mixtures incorporating different types of cementitious fillers.

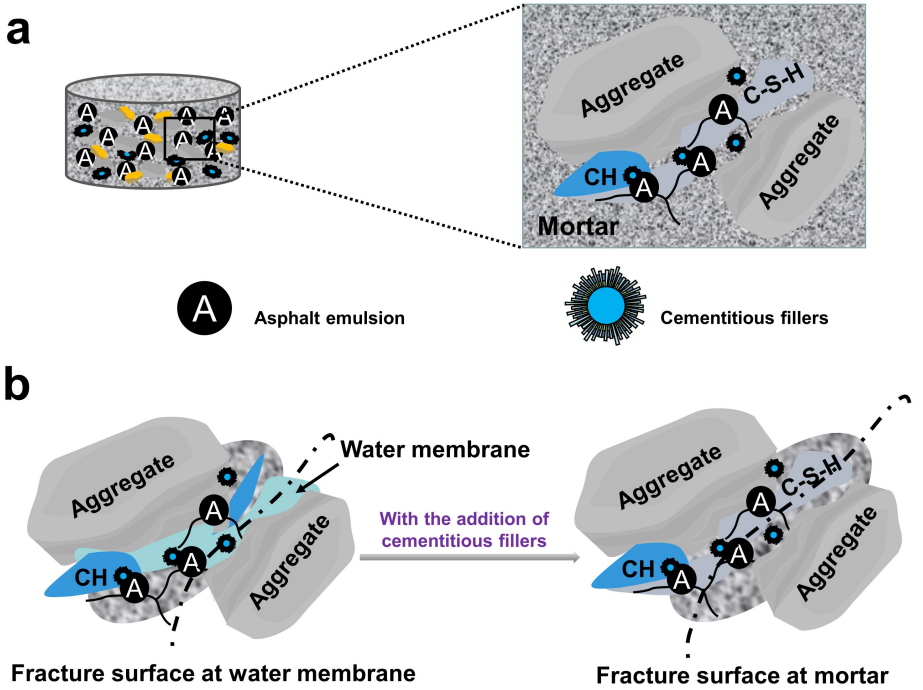

Fig. 6. Schematic illustration of (a) the formation of additional hydration products in the interface area and (b) the mechanism of strength formation in CMA with the addition of cementitious fillers.

3.1.2. Raveling loss

We then performed the raveling loss test of all produced CMA mixtures. Fig. 7 plots the raveling loss values of the CMA sample incorporating different types of fillers. As can be seen, the raveling

loss of the CMA samples first decreased and then increased with the increase of the OPC content. The CMA-6% OPC mix demonstrated a 21.8% raveling loss, slightly higher than the CMA-2% OPC or CMA-4% OPC sample, suggesting that the admixed OPC could reduce the raveling loss of CMA without OPC, but there might exist an optimum OPC content (~4%). This was mainly due to the overdose of OPC that introduced in CMA could result in a higher number of air voids (Zhu et al., 2019b).

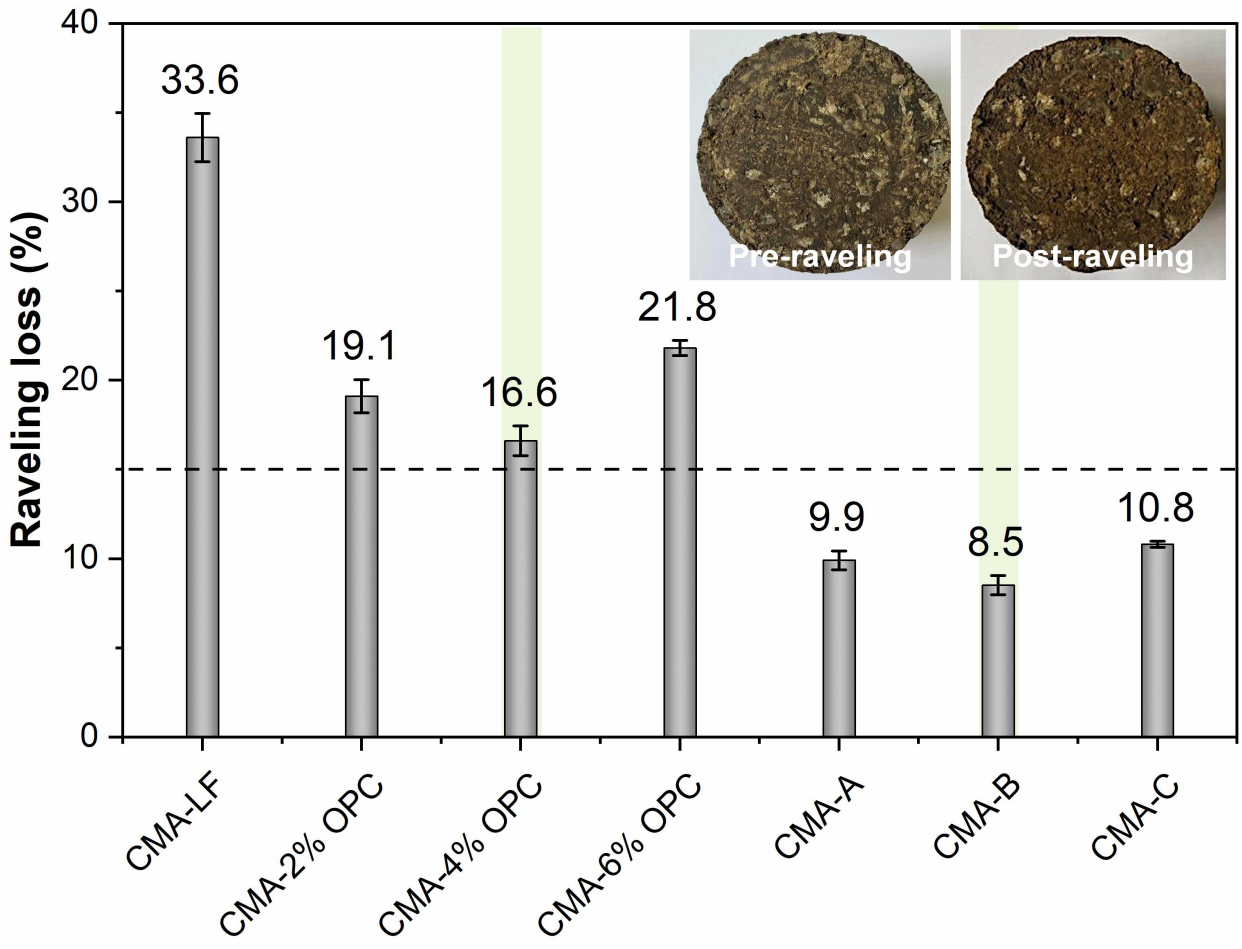

Fig. 7. Raveling loss of the CMA mixtures containing different types of fillers. Inset is the CMA-B specimen before and after the raveling test.

On the other hand, with the addition of ternary blended cementitious fillers, the raveling loss values of the CMA samples were considerably decreased to a level below 15%. Especially for the CMA-B mix, which contains 2% OPC, 1% FA, and 1% GGBS, its raveling loss decreased to 8.5%. This

237 result can be attributed, to a great extent, to outstanding strength and thus obtain good integrity and
238 cohesiveness (Wang, Z. et al., 2020; Xiao et al., 2019). Based on the visual observation, indeed, the
239 CMA-B sample maintained a relatively complete structure after the raveling test (see inset). It can
240 be concluded that using ternary blended cementitious fillers can greatly improve the abrasion
241 resistance of CMA caused by early-age traffic.

242 *3.2. Engineering performance*

243 Engineering performance can directly reflect the impact of the external loading and environment on
244 CMA during its service life (Nassar et al., 2016; Wang et al., 2015; Yan et al., 2017). As such, we
245 performed moisture susceptibility, rutting resistance, and cracking susceptibility tests of all
246 produced CMA samples, aiming to provide a deep understanding of the field performance of the
247 CMA mixture.

248 *3.2.1. Moisture susceptibility*

249 Fig. 8 presents the RS and TSR values of CMA containing different types of fillers. As can be seen,
250 the RS and TSR values both increased with the OPC content and reached their maximum value at
251 6% OPC content. For the CMA-LF without OPC, its RS value was only 69.3%. When 2% OPC was
252 added as the cementitious filler (CMA-2% OPC), the RS value significantly increased to 85.6%.
253 Similarly, the CMA-6% OPC demonstrated a higher RS value of 83.8% and a TSR value of 91.8%.
254 Similar conclusions have been confirmed by others reports (Tian et al., 2020a; Xiao et al., 2019).
255 The benefits of the introduction of OPC increased the number of hydration products with high
256 resistance to water damage, which also has the ability to reduce the voids and increase the density
257 of the CMA.

Significantly, the RS values further increased to approximately 95% for the CMA specimens containing ternary blended cementitious fillers, almost 35% higher than that of the sample without cementitious filler. Since the improvement of the bond strength between the aggregate and mortar (Dong et al., 2018; Xiao et al., 2019) in the CMA mixture with the addition of cementitious fillers, the CMA-B mix obtained the highest TSR value in that case, superior to the corresponding sample CMA-LF with the TSR value of 65.78%. Consistent with the results of the indirect tensile tests, the RS results of this study strongly suggest that the ternary blended cementitious fillers could increase the interaction between aggregate and mortar (see Fig. 6), thus leading to enhanced water stability of CMA.

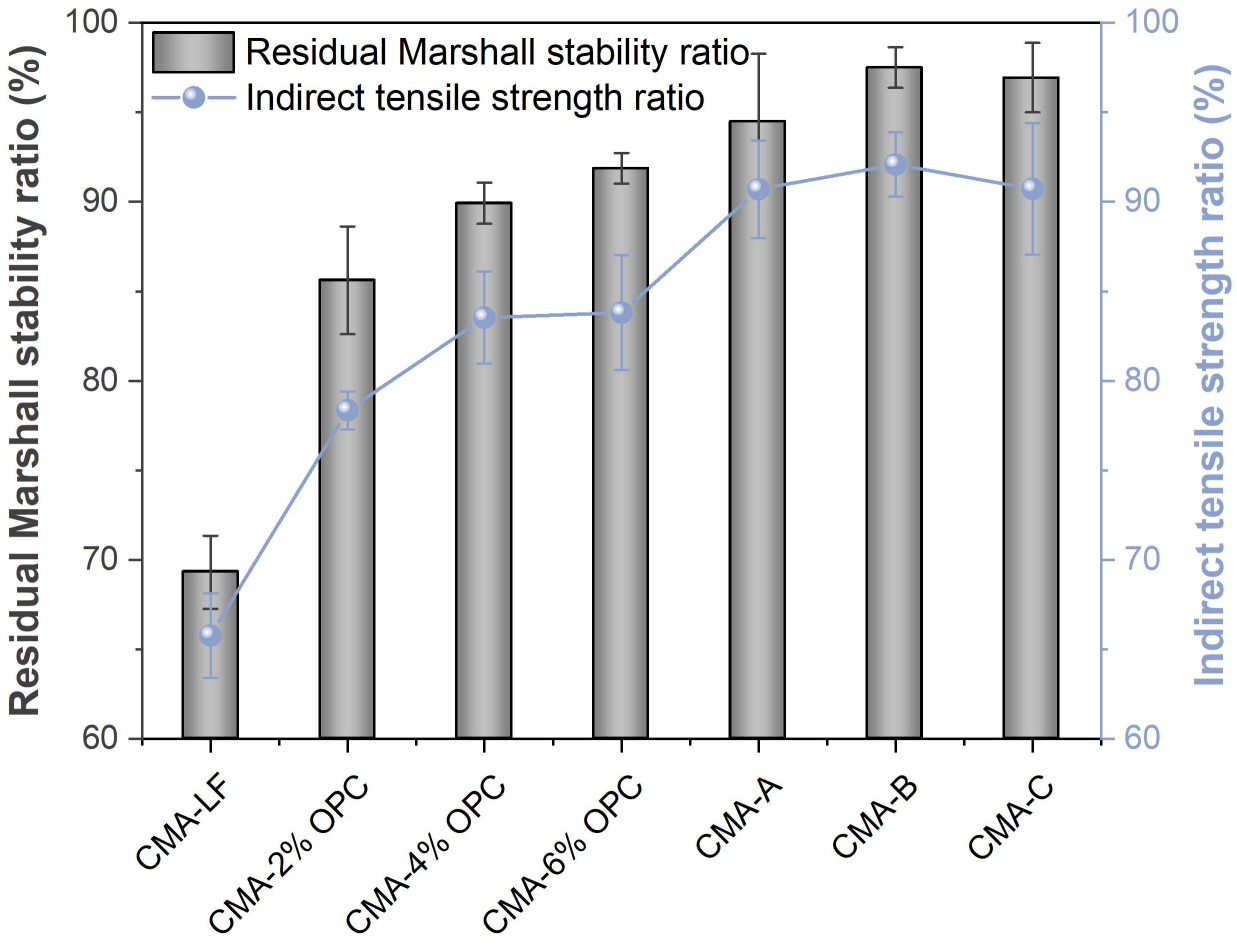

Fig. 8. Moisture stability of the CMA mixtures containing different types of fillers.

3.2.2. Rutting resistance at high-temperature

Fig. 9 depicts the DS values of slab samples tested at high temperatures. As can be seen, the DS values improvement was proportional to the OPC content. The reinforcing effect of rutting resistance was most obvious with the addition of 6% OPC content, which was considerably higher than that of the CMA-LF mix, with which the DS value increased by approximately 8 times. This result can be ascribed, to a great extent, the admixed OPC accelerated the demulsification of asphalt emulsion. Meanwhile, the water existing in the asphalt emulsion could promote cement hydration. In consequence, asphalt films and hydration products could be connected to form a network structure to provide excellent resistance to deformation, which will be further discussed in Section 3.3.2.

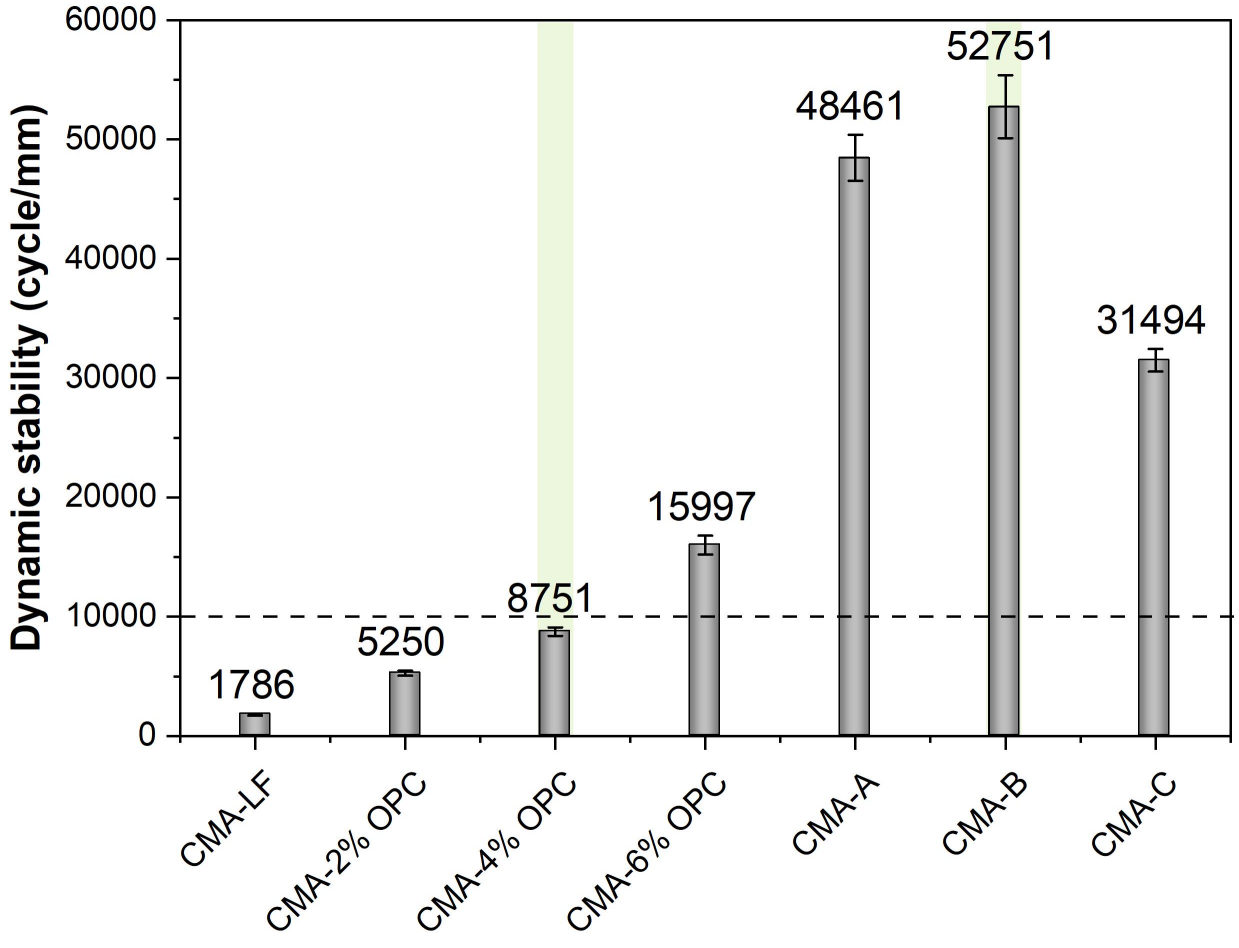

Fig. 9. Dynamic stability of the CMA specimens containing different types of fillers.

On the other hand, partial replacement of OPC either by FA or GGBS (CMA-A, CMA-B, and CMA-C) can significantly increase the DS values. For instance, the DS value drastically increased to 52751 cycle/mm for the CMA-B mix, with which the DS value was approximately 10 times that of the CMA-2% OPC. The remarkable DS values we achieved should be attributed to the reduction of voids and enhancement of strength for the CMA mixture. Moreover, the density of CMA has increased and resulted in less vertical deformation. The positive influence of combining the usage of fillers on the rutting resistance of CMA was revealed, which had a considerably longer life under high-temperature than the CMA-LF mix. For improving the rutting resistance of CMA, the order of ternary blended cementitious fillers was CMA-B > CMA-A > CMA-C. This indicates that there are some synergistic effects among these cementitious fillers and the CMA-B mix is believed to be suitable for applications in road pavements subjected to harsh service conditions in terms of high temperature.

3.2.3. Low-temperature cracking susceptibility

The bending strength, bending failure strain, and bending creep stiffness values are presented in Fig. 10. It is well known that higher bending failure strain was associated with lower bending creep stiffness and better crack resistance (Wang, Z. et al., 2020; Xiao et al., 2019). As suggested in Fig. 10b, the CMA-LF mix had the highest bending failure strain and the lowest bending creep stiffness. When 6 wt% OPC was added, the bending strength of the mixtures increased by approximately 20% (Fig. 10a), whereas the bending failure strain decreased by approximately 15% (Fig. 10b). This is expected because the admixing cement increased the density and stiffness of the mixtures. Additionally, the bending creep stiffness could further be increased to about 2900 MPa for CMA-B,

298 which is about 1.1 times higher than that of the CMA-2% OPC mix. These findings, together with
299 the rutting resistance results, may indicate that the admixed ternary blended cementitious fillers
300 adversely affect the crack resistance of CMA at low-temperature.

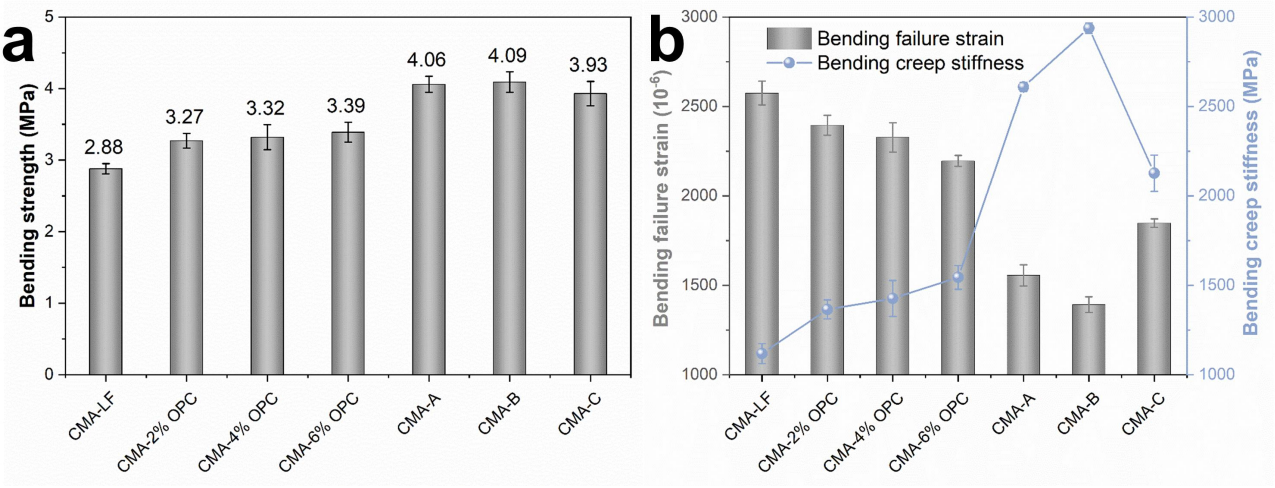

Fig. 10. Cracking susceptibility of the CMA mixtures: (a) bending strength and (b) bending failure strain and bending creep stiffness.

301 *3.3. Microscopic investigation*

302 To understand the origin of the improvement in early age road performance, as well as the
303 underlying strengthening mechanism of the admixed blended cementitious fillers, we studied the
304 composition and microstructure of produced CMA mortars using various characterization
305 techniques.

306 *3.3.1. XRD and FTIR analysis*

307 Fig. 11a demonstrates the XRD patterns of the hardened CMA mortar samples. The crystallography
308 open database (COD) was cited for XRD analysis in this study. Although exact quatitation using
309 XRD is difficult, semi-quantitative analysis of the hydration products is possible by comparing a
310 large amount of peak intensity data (Birenboim et al., 2019; Tafesse and Kim, 2019).

311 The typical reflections, e.g., portlandite, alite, and belite can be detected in CMA samples. As one of

the major crystalline phases produced from the hydration process of cementitious fillers (Tan et al., 2013), the intensities of portlandite peaks located at 18.2°, 34.1°, 47.2°, and 50.1° were observed. To intuitively reflect the roles of cementitious fillers in CMA, in this study, only the characteristic peaks of portlandite (P), alite (A), and belite (B) were marked in XRD patterns. The diffraction peak of portlandite was found in the CMA-4% OPC mix, but not detected in the CMA-LF mix. A higher diffraction intensity and larger peak area of portlandite were observed in the CMA-B mix. On the other hand, the CMA-B sample demonstrated the weakest diffraction peaks of alite and belite, which further confirmed that using ternary blended cementitious fillers could participate in the hydration reactions, promote the generation of hydration crystals, and has the potential to gain strength for CMA.

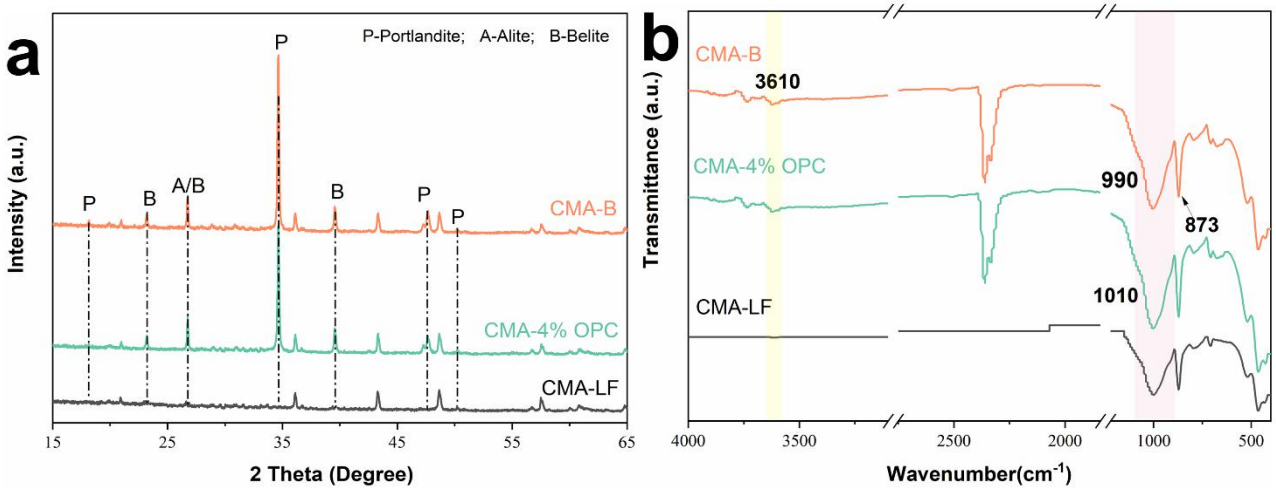

Fig. 11. Composition analysis of the hardened CMA mortars: (a) XRD patterns and (b) FTIR curves (only the characteristic bands of O-H, Si-O-Si, and Al-O-Si were marked).

As can be seen, the bands at 990-1010 cm^{-1} in CMA were attributed to the asymmetric stretching vibrations of Al-O-Si or Si-O-Si (Wang, J. et al., 2020), implying that the formation of amorphous to semi-crystalline alumina-silicate materials (Saride et al., 2016). Interestingly, this peak shifted from 1010 cm^{-1} in the CMA-4% OPC sample to 990 cm^{-1} in the CMA-B sample. It is known that in this region, these peaks and their area directly indicate the number of hydration products (Saride et

al., 2016). The intensity of O-H bands around 3610 cm^{-1} in the CMA-2% OPC or CMA-B sample was stronger than that of the CMA-LF mix. Moreover, the band around 873 cm^{-1} was also observed in the CMA-B sample and a higher peak area further confirmed that hydration products have been generated, which can also be supported by the previous XRD analysis (Fig. 11a).

3.3.2. Microstructure observation

The SEM images in Fig. 12a show that for the sample of CMA-LF, there are a large number of voids with asphalt films discontinuously distributed. Thus, the CMA-LF sample demonstrated a loose microstructure and lower strength (see Section 3.1). Further amplification, the surface of the hardened CMA specimen was not smooth and showed many uneven protrusions, which were randomly distributed in the cement-asphalt matrix (Fig. 12b). According to the EDS analysis, it can be inferred that the uneven protrusions were asphalt particles (Fig. 12c).

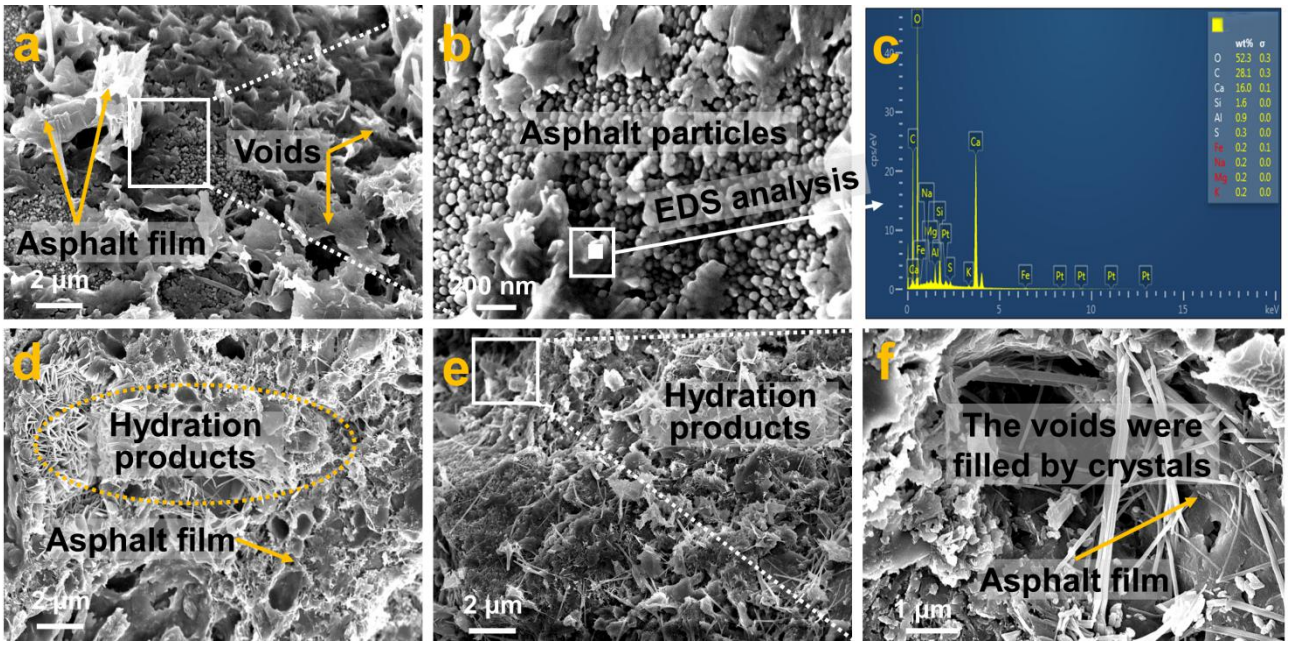

Fig. 12. Selective SEM images of CMA samples: (a) CMA-LF, (b) SEM image of the box in (a) with high magnification, (c) EDS analysis of the uneven protrusions in (b), (d) CMA-4% OPC, (e) CMA-B, (f) SEM image of the box in (e) with high magnification.

The SEM image of the CMA-4% OPC sample shows, a dense microstructure with several cement

hydrates was formed (Fig. 12d). The reason for the dense structure was that these hydration products and asphalt films were partially formed the network structure, which provided a certain strength in CMA. For the CMA-B sample, it can be observed that the microstructure was more uniform and dense (Fig. 12e). Moreover, the regular and compact microstructure was composed mainly of the C-S-H phase. Further amplification, some needle-like crystals have filled the voids left by water evaporation in CMA can be observed in the CMA-B sample (Fig. 12f), while it does not found in CMA-LF or CMA-4% OPC sample. Moreover, the original large voids were divided into several small voids, and some crystals even penetrated the asphalt film. Suggesting the composites of cement hydrates and asphalt film with interpenetrating networks provided excellent strength and helped to improve the engineering property of the mixture. The visible densification of microstructure provides a rational explanation of the remarkable performance of CMA mixtures in early-age strength tests (Figs. 5 and 7) and dynamic stability test (Fig. 9).

Overall, using ternary blended cementitious fillers can enhance the early-age strength of CMA to meet open traffic requirements. The engineering performance results suggest that the ternary blended cementitious fillers could be suitable for applications in road pavements subjected to harsh service conditions in terms of moisture and high temperature, mainly due to the enhanced interface bonding between aggregate and matrix, reduced air voids, and regulated the microstructure.

4. Conclusions

This laboratory study has developed a novel CMA incorporating ternary blended cementitious fillers that feature remarkably improved strength and microstructure. Based on the results of early-age strength testing, engineering performance testing, XRD, FTIR, and SEM-EDS, the following conclusions can be drawn:

(1) Admixing ternary blended cementitious fillers greatly enhanced the early-age strength of CMA. In particular, the ITS of CMA-B in this study has increased by about 20%, as compared to the 2% OPC content group, simultaneously, the raveling loss has decreased by about 55%, indicating that this design route can be successfully used to manufacture CMA with outstanding early-age strength.

(2) The addition of 2% OPC, 1% FA, and 1% GGBS to CMA resulted in a significant improvement of DS value up by 10 times, the rutting resistance outperformed previously reported CMA containing cementitious fillers. Simultaneously, the improvement in the interface between aggregate and matrix, as well as the reduction of air voids, both contribute to the strength formation and provide reliable water stability, and thus suitable for applications in road pavements subjected to harsh service conditions in terms of moisture and temperature.

(3) The admixed ternary blended cementitious fillers have participated in the hydration reactions and conducive to the demulsification of asphalt emulsion, thus resulting in much more hydration products, as well as regular and compact microstructure. Simultaneously, a higher density mixture with fewer air voids has been achieved, which explains the improvement of CMA in strength. However, the cracking susceptibility has been slightly compromised because of the formation of the matrix with excellent stiffness.

(4) This laboratory study has demonstrated great potential to reduce the cement consumption in CMA fabrication, thus mitigating the environmentally harmful impacts and making CMA even cleaner. The next steps will be employed at the construction site and we recommend employing ternary blended cementitious fillers to improve the early road performance of CMA.

Declaration of competing interest

The authors declare that they have no known competing financial interests or personal relationships

that could have appeared to influence the work reported in this paper.

CRediT authorship contribution statement

Dong Lu: Writing-Original Draft, Writing-Review and Editing, Data curation. **Jian Yuan**: Visualization, Conceptualization, Writing-Review and Editing. **Zhen Leng**: Writing-Review and Editing, Supervision. **Jing Zhong**: Investigation, Writing-Review and Editing, Supervision, Funding acquisition.

Acknowledgments

The authors owe their thanks to Dr. Zhenliang Jiang at Ryerson University for his assistance in the image analysis. The authors thank Mr. Baobao Yan for his assistance in the use of the Fourier Transform Infrared Spectrometer.

References

Al-Khateeb, G.G., Al-Akhras, N.M., 2011. Properties of Portland cement-modified asphalt binder using Superpave tests. Construction and Building Materials 25(2), 926-932.http://dx.doi.org/10.1016/j.conbuildmat.2010.06.091

Ayar, P., 2018. Effects of additives on the mechanical performance in recycled mixtures with bitumen emulsion: An overview. Construction and Building Materials 178, 551-561.http://dx.doi.org/10.1016/j.conbuildmat.2018.05.174

Birenboim, M., et al., 2019. Reinforcement and workability aspects of graphene-oxide-reinforced cement nanocomposites. Composites Part B: Engineering 161, 68-76.http://dx.doi.org/10.1016/j.compositesb.2018.10.030

Bołtryk, M., Małaszkiewicz, D., 2013. Application of anionic asphalt emulsion as an admixture for concrete. Construction and Building Materials 40, 556-565.http://dx.doi.org/10.1016/j.conbuildmat.2012.11.110

Diaz, L.G., 2016. Creep performance evaluation of Cold Mix Asphalt patching mixes. International Journal of Pavement Research and Technology 9(2), 149-158.http://dx.doi.org/10.1016/j.ijprt.2016.04.002

Dodds, W., et al., 2017. Durability performance of sustainable structural concrete: Effect of coarse crushed concrete aggregate on rapid chloride migration and accelerated corrosion. Construction and Building Materials 155, 511-521.http://dx.doi.org/10.1016/j.conbuildmat.2017.08.073

Dolzycki, B., et al., 2017. The long-term properties of mineral-cement-emulsion mixtures. Construction and Building Materials 156, 799-808.http://dx.doi.org/10.1016/j.conbuildmat.2017.09.032

Dołżycki, B., et al., 2017. The Influence of Binding Agents on Stiffness of Mineral-cement-emulsion Mixtures. Procedia Engineering 172, 239-246.http://dx.doi.org/10.1016/j.proeng.2017.02.103

Dong, Q., et al., 2018. Reduction of moisture susceptibility of cold asphalt mixture with Portland cement and bentonite nanoclay additives. Journal of Cleaner Production 176, 320-328.http://dx.doi.org/10.1016/j.jclepro.2017.12.163

Doyle, T.A., et al., 2013. Developing maturity methods for the assessment of cold-mix bituminous materials. Construction and Building Materials 38, 524-529.http://dx.doi.org/10.1016/j.conbuildmat.2012.09.008

Du, S., 2018. Effect of curing conditions on properties of cement asphalt emulsion mixture. Construction and Building Materials 164, 84-93.http://dx.doi.org/10.1016/j.conbuildmat.2017.12.179
Dulaimi, A., et al., 2016. New developments with cold asphalt concrete binder course mixtures containing binary blended cementitious filler (BBCF). Construction and Building Materials 124, 414-423.http://dx.doi.org/10.1016/j.conbuildmat.2016.07.114
Dulaimi, A., et al., 2017. High performance cold asphalt concrete mixture for binder course using alkali-activated binary blended cementitious filler. Construction and Building Materials 141, 160-170.http://dx.doi.org/10.1016/j.conbuildmat.2017.02.155
Dulaimi, A., et al., 2020. The mechanical evaluation of cold asphalt emulsion mixtures using a new cementitious material comprising ground-granulated blast-furnace slag and a calcium carbide residue. Construction and Building Materials 250.http://dx.doi.org/10.1016/j.conbuildmat.2020.118808
Ferrotti, G., et al., 2014. Experimental characterization of high-performance fiber-reinforced cold mix asphalt mixtures. Construction and Building Materials 57, 117-125.http://dx.doi.org/10.1016/j.conbuildmat.2014.01.089
Ge, Z., et al., 2015. Properties of cold mix asphalt mixtures with reclaimed granular aggregate from crushed PCC pavement. Construction and Building Materials 77, 404-408.http://dx.doi.org/10.1016/j.conbuildmat.2014.12.084
Leandri, P., et al., 2015. Field validation of recycled cold mixes viscoelastic properties. Construction and Building Materials 75, 275-282.http://dx.doi.org/10.1016/j.conbuildmat.2014.11.028
Lin, J., et al., 2017. Dynamic characteristics of 100% cold recycled asphalt mixture using asphalt emulsion and cement. Journal of Cleaner Production 156, 337-344.http://dx.doi.org/10.1016/j.jclepro.2017.04.065
Ling, C., et al., 2016. Measuring moisture susceptibility of Cold Mix Asphalt with a modified boiling test based on digital imaging. Construction and Building Materials 105, 391-399.http://dx.doi.org/10.1016/j.conbuildmat.2015.12.093
Lu, D., et al., 2020. Effects of Combined Usage of Supplementary Cementitious Materials on the Thermal Properties and Microstructure of High-Performance Concrete at High Temperatures. Materials (Basel) 13(8).http://dx.doi.org/10.3390/ma13081833
Martínez-Echevarría, M.J., et al., 2012. In-laboratory compaction procedure for cold recycled mixes with bituminous emulsions. Construction and Building Materials 36, 918-924.http://dx.doi.org/10.1016/j.conbuildmat.2012.06.040
Mignini, C., et al., 2021. Using fine aggregate matrix mortars to predict the curing behaviour of cement bitumen treated materials produced with different cements. Construction and Building Materials 268.http://dx.doi.org/10.1016/j.conbuildmat.2020.121201
Moghadas Nejad, F., et al., 2017. Investigating the mechanical and fatigue properties of sustainable cement emulsified asphalt mortar. Journal of Cleaner Production 156, 717-728.http://dx.doi.org/10.1016/j.jclepro.2017.04.105
Nassar, A.I., et al., 2016. Mechanical, durability and microstructure properties of Cold Asphalt Emulsion Mixtures with different types of filler. Construction and Building Materials 114, 352-363.http://dx.doi.org/10.1016/j.conbuildmat.2016.03.112
Saadoon, T., et al., 2018. Prediction of water evaporation and stability of cold asphalt mixtures containing different types of cement. Constr. Build. Mater. 186, 751-761.http://dx.doi.org/10.1016/j.conbuildmat.2018.07.218
Saride, S., et al., 2016. Micro-mechanical interaction of activated fly ash mortar and reclaimed asphalt pavement materials. Construction and Building Materials 123, 424-435.http://dx.doi.org/10.1016/j.conbuildmat.2016.07.016
Tafesse, M., Kim, H.-K., 2019. The role of carbon nanotube on hydration kinetics and shrinkage of cement composite. Composites Part B: Engineering 169, 55-64.http://dx.doi.org/10.1016/j.compositesb.2019.04.004
Tan, Y., et al., 2013. Effect of emulsifier on cement hydration in cement asphalt mortar. Construction and Building Materials 47, 159-164.http://dx.doi.org/10.1016/j.conbuildmat.2013.04.044
Tian, Y., et al., 2020a. Effects of cement contents on the performance of cement asphalt emulsion mixtures with rapidly developed early-age strength. Construction and Building Materials 244.http://dx.doi.org/10.1016/j.conbuildmat.2020.118365

Tian, Y., et al., 2020b. Characteristics of the Cement Asphalt Emulsion Mixture With Early-Age Strength and Flowability. Frontiers in Materials 7.http://dx.doi.org/10.3389/fmats.2020.00122

Wang, J., et al., 2020. Thinner fillers, coarser pores? A comparative study of the pore structure alterations of cement composites by graphene oxides and graphene nanoplatelets. Composites Part A: Applied Science and Manufacturing 130.http://dx.doi.org/10.1016/j.compositesa.2019.105750

Wang, Z., et al., 2020. Early-stage road property improvements of cold recycled asphalt emulsion mixture with microwave technology. Journal of Cleaner Production 263.http://dx.doi.org/10.1016/j.jclepro.2020.121451

Wang, Z., et al., 2015. Effects of asphalt emulsion on properties of fresh cement emulsified asphalt mortar. Construction and Building Materials 75, 25-30.http://dx.doi.org/10.1016/j.conbuildmat.2014.11.013

Xiao, J., et al., 2019. Effect of cement and emulsified asphalt contents on the performance of cement-emulsified asphalt mixture. Construction and Building Materials 220, 577-586.http://dx.doi.org/10.1016/j.conbuildmat.2019.06.051

Yan, J., et al., 2017. Early-age strength and long-term performance of asphalt emulsion cold recycled mixes with various cement contents. Construction and Building Materials 137, 153-159.http://dx.doi.org/10.1016/j.conbuildmat.2017.01.114

Yan, J., et al., 2014. The theoretical analysis of the RAP aged asphalt influence on the performance of asphalt emulsion cold recycled mixes. Construction and Building Materials 71, 444-450.http://dx.doi.org/10.1016/j.conbuildmat.2014.09.002

Yan, X., et al., 2019. Evaluation of sulfate resistance of slag contained concrete under steam curing. Construction and Building Materials 195, 231-237.http://dx.doi.org/10.1016/j.conbuildmat.2018.11.073

Zhu, C., et al., 2019a. Effect of gradations on the final and long-term performance of asphalt emulsion cold recycled mixture. Journal of Cleaner Production 217, 95-104.http://dx.doi.org/10.1016/j.jclepro.2019.01.264

Zhu, C., et al., 2019b. Long-term performance and microstructure of asphalt emulsion cold recycled mixture with different gradations. Journal of Cleaner Production 215, 944-951.http://dx.doi.org/10.1016/j.jclepro.2019.01.103